Potential landscapes and induced charges near metallic islands in three dimensions

A. Weichselbaum and S. E. Ulloa
Department of Physics and Astronomy, and Nanoscale and Quantum Phenomena Institute, Ohio University, Athens, Ohio 45701, USA

(Received 23 June 2003; published 25 November 2003)

We calculate electrostatic potential landscapes for an external probe charge in the presence of a set of metallic islands. Our numerical calculation in three dimensions (3D) uses an efficient grid relaxation technique. The well-known relaxation algorithm for solving the Poisson equation in two dimensions is generalized to 3D. In addition, all charges on the system, free as well as induced charges, are determined accurately and self-consistently to satisfy the desired boundary conditions. This allows the straightforward calculation of the potential on the outer boundary using the free space electrostatic Green's function, as well as the calculation of the entire capacitance matrix of the system. Physically interesting examples of nanoscale systems are presented and analyzed.

DOI: 10.1103/PhysRevE.68.056707 PACS number(s): 02.70.−c, 41.20.−q

I. INTRODUCTION

There is a need to precisely know the electrostatic landscape experienced by electrons in ever smaller structures, down to the scale of scanning tunnelling microprobes (STM) and single electron devices. The presence of conducting leads for manipulating and measuring local potentials influences the quantum mechanical behavior of electrons in a highly nontrivial manner. In polarizable media, for example, charged ''conglomerates'' which include free as well as polarization charges in the neighborhood, behave as quasiparticles which can live for a comparatively long time and interact with the conducting leads via Coulomb interaction. Knowledge of the potential landscape describing this interaction for the case of a quasiparticle is an interesting and important element in the better understanding of these systems. Electrons in single-electron transistors [1], or moving in the neighborhood of lithographically defined gate arrangements [2], or tunnelling through STM scanning tips are but a few examples of the pervasiveness of electrostatic potentials in realistic structures.

The solution of the Laplace or Poisson equation to obtain electrostatic potential landscapes is a well defined boundary value problem, typically requiring the discretization of space on a convenient grid. Relaxation techniques are well known [3–5] and widely used in the solution of these problems, as they provide convenient and efficient algorithms [6]. For dimensions lower than three, simple second order algorithms are used together with common speedup features such as successive over-relaxation (SOR) and Gauss-Seidel (GS) iteration schemes [3,4]. In three dimensions (3D), however, due to the poor scaling with grid dimensions, more efficient routines are desirable. In this context a generalized $O(h^6)$ algorithm for 3D is presented in this paper, and used to calculate the potential landscape of several physical systems of interest, as those mentioned above.

The boundary conditions most easily built into relaxation algorithms are fixed voltage surfaces, with the voltage known and provided by an external battery, for example. This does not apply, however, to cases with a *floating* potential, such as metallic islands which are isolated from the environment (like metallic quantum dots), or for open boundary problems. In the case of isolated islands, the value of the potential at a metallic boundary, even though constant, is not known. On the other hand, the overall charge on the island is determined at the outset and can be considered to be known. The solution to the problem taken here is that once one has access to the linear relationship between the charge on the island and the island potential derived from the relaxation algorithm, one can invert this relationship and calculate the potential with every relaxation cycle such that the overall charge is maintained at a fixed value, e.g., zero for an overall neutral island. Incorporation of this idea in the iteration procedure yields the appropriate floating potentials, as we will show.

Note moreover that the outer boundary is open in general in most nanosized geometries. If the size of the calculated cell could be chosen large enough, of course, one could assume that the potential would drop to zero there; however, this is operationally forbidden by the vast number of grid points needed in that case. The only feasible way is to determine the nonuniform potential on the outer boundary self-consistently within the algorithm. The approach taken in this paper is that the knowledge of the total charge distribution (external *and* induced charges) allows for the calculation of the potential on the outer boundary via the standard free-space electrostatic Green's function, $1/4\pi r$. This is a straightforward if computationally expensive procedure, which can be speeded up remarkably by tabulating the inverse distances on the grid, but yields physically well-behaved asymptotics in all cases, as we will see. We should also emphasize that once the charges and potentials in the system are known, one can easily evaluate the capacitance matrix for the geometries of interest, regardless of the symmetries of the arrangement.

The remainder of the paper describes the algorithm in detail in Sec. I, while Sec. II illustrates its use in several physically relevant examples.

II. ALGORITHM

Taking the standard Taylor expansion of a smooth function $f(x,y,z)$ around each grid point, one defines the *center*

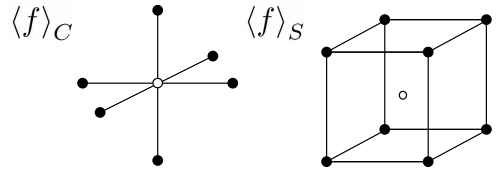

FIG. 1. Visualization of averages taken on the grid: average $\langle f \rangle_C$ as in Eq. (1a) is over nearest neighbors (NN); average $\langle f \rangle_S$ as in Eq. (1b) is over third nearest neighbors (TNN). The grid points included in the sum are shown as filled symbols; solid lines joining these have length of two grid spacings, $2h$.

average and the *square average* as follows (assuming uniform grid spacing h in all three dimensions)

$$\langle f \rangle_C \equiv \frac{1}{6}\left(\sum_{i,j,k}^{\mathrm{NN}} f_{ijk} \right) = f^{(000)} + \frac{h^2}{6}\vec{\nabla}^2 f + \frac{h^4}{72}(f^{(400)} + f^{(040)} + f^{(004)}) + O(h^6), \tag{1a}$$

$$\langle f \rangle_S \equiv \frac{1}{8}\left(\sum_{i,j,k}^{\mathrm{TNN}} f_{ijk} \right) = f^{(000)} + \frac{h^2}{2}\vec{\nabla}^2 f + \frac{h^4}{24}(f^{(400)} + f^{(040)} + f^{(004)}) + \frac{h^4}{4}(f^{(220)} + f^{(202)} + f^{(022)}) + O(h^6), \tag{1b}$$

where (T)NN stands for (third) nearest neighbors and

$$f^{(rst)} \equiv \frac{\partial^r}{\partial x^r}\frac{\partial^s}{\partial y^s}\frac{\partial^t}{\partial z^t} f(i,j,k), \tag{2a}$$

$$f_{\mathbf{i}} \equiv f_{ijk} \equiv f(i,j,k) \equiv f(ih,jh,kh), \tag{2b}$$

with i, j, k and r, s, t being integers. The averages in Eqs. (1) are shown graphically in Fig. 1. Note that the odd-order derivatives in Eqs. (1) cancel due to the symmetric combinations around the grid points included in the averages. Also note that *second* (or next) nearest neighbors are considered in the ''checkered lattice'' sweeps of the points making the simple cubic grid. (The relaxation sweeps are done sequentially over the face-centered cubic array of neighbors which form effectively a dual lattice.)

Taking the linear combination of the averages of Eqs. (1a) and (1b)

$$\langle\langle f \rangle\rangle \equiv \alpha \langle f \rangle_C + (1-\alpha)\langle f \rangle_S, \tag{3}$$

then with $\alpha \equiv \alpha_{3D} = 6/7$ the *overall average* becomes

$$\langle\langle f \rangle\rangle_{3D} = f_{\mathbf{i}} + \tfrac{3}{14}h^2\vec{\nabla}^2 f_{\mathbf{i}} + \tfrac{1}{56}h^4\vec{\nabla}^2\vec{\nabla}^2 f_{\mathbf{i}} + O(h^6). \tag{4}$$

Since we are solving for the Poisson equation

$$\vec{\nabla}^2 f = -g, \tag{5}$$

Eq. (4) can be rewritten as

$$f_{\mathbf{i}} = \langle\langle f \rangle\rangle_{3D} + \tfrac{3}{28}h^2(g_{\mathbf{i}} + \langle g \rangle_C) + O(h^6), \tag{6}$$

where $\langle g \rangle_C$ is the *center average* for the *source term* at a given grid point. Equation (6), together with Eq. (4), serves as the basis for the iterative scheme: the potential f is *relaxed to its minimum* considering external sources g and the potential of the (third and) nearest neighbor sites through the linear three-dimensional average. In order to calculate charges on the grid, Eq. (4) is employed again and gives a straightforward way for calculating *real* (i.e., free) and *induced* charges on the grid on an equal footing. Thus using Poisson's Eq. (5), the charge contribution of each grid point can be calculated as follows

$$q_{\mathbf{i}} \equiv h^3 g_{\mathbf{i}} = h(-h^2\vec{\nabla}^2 f_{\mathbf{i}}) = \tfrac{14}{3}h[f_{\mathbf{i}} - \langle\langle f \rangle\rangle_{3D} + O(h^4)]. \tag{7}$$

For convenience, throughout the paper we adopt the following convention on units. The charge of an electron e is set to 1; therefore the electric potential is the same as the potential energy. The Coulomb energy is written in units of eV as $E = q_1[e]q_2[e]/(4\pi r)$ which straightforwardly implies a unit for the distance of $[r] = 18.1$ nm. Summarizing, the units chosen are

$$[\mathrm{charge}] = e;\ [\mathit{energy}] = \mathrm{eV};\ [\mathrm{distance}] = 18.1\ \mathrm{nm}. \tag{8}$$

Therefore, taking these units, brings one naturally into the realm of nanostructures.

A. Successive over relaxation and iteration scheme

The general method for SOR is described for 2D in Refs. [3,4] for a $N \times N$ array, and generalized here to 3D as given by

$$f_{\mathbf{i}}^{(i+1)} = f_{\mathbf{i}}^{(i)} + \omega(f_{\mathbf{i}}^{(new)} - f_{\mathbf{i}}^{(i)}), \tag{9a}$$

where

$$\omega = \frac{2}{1 + \pi/\min(N_x, N_y, N_z)}, \tag{9b}$$

N_j is the grid size in the jth direction, and $f_{\mathbf{i}}^{(new)}$ is calculated according to Eq. (6). The SOR parameter ω is in the range $1 < \omega < 2$ as required for the algorithm to converge. The basic idea behind ω is that if one is heading in the *right* direction (e.g., towards the solution), why not go a bit further. An ω too large ($\omega > 2$), however, results in instability of the algorithm and the relaxation process overshoots and diverges. Equation (9b) was tested for different N_x, N_y, and N_z values and it was indeed this specific combination that gave the optimal value for ω (note that the window for a *good* ω is quite narrow in general). The specific structure of Eq. (9b) can be intuitively understood as follows: the SOR algorithm introduces perturbations in the system that propagate during the relaxation cycles and eventually die out if the grid is large enough; however, for finite grid sizes, the perturbations are reflected at the boundaries and so they interfere and pile up. In this sense, the minimum extension within the three grid dimensions constrains the optimal magnitude of ω, consistent with Eq. (9b).

For further optimization of the algorithm, the Gauss-Seidel iteration scheme was adopted, as well as the alternating relaxation on the two checkerboard like subgrids that in

sum span the whole grid [3,4]. The *inverse* distances between the grid points were mapped into a table, such that the calculation of the potential in the grid is sped up remarkably. According to Coalson [6], multigrid methods can be applied to account for the slowly converging long wavelength portions of the solution. This was not done here, since the variation of the potential on the isolated islands and especially the calculation of the outer boundary already introduced longer range correlations over the grid that presumably made the algorithm converge faster in our case.

A note about efficiency: As we use a successive overrelaxation method to iterate the potential on the grid, the total relaxation time for this in 2D is proportional to $\sim n^{3/2}$, where n is the *total* number of grid points [4], and is thus clearly comparable to algorithms like conjugate gradient. Also note that SOR has still known improvements that may also be implemented and would thus make this algorithm superior to the former [4]. Our relaxation over the bipartite lattices composing the simple cubic three-dimensional grid preserves the spirit of the two-dimensional algorithms, but obtains an accuracy of $O(h^6)$, as discussed above.

B. Open outer boundary

Equation (7) gives a consistent higher order recipe for calculating the overall charge distribution, including induced as well as the external (free) charges [7,8], given via the source term g in the Poisson equation (5). Starting with an (arbitrary) initial constant potential on the outer boundary (OB), these values are updated every time the interior of the grid has relaxed down to a certain accuracy level ε,

$$V_{\mathbf{i}}^{OB}=\frac{1}{4\pi}\sum_{q_{\mathbf{j}}\neq 0} q_{\mathbf{j}}(d^{-1})_{\mathbf{ij}},$$

and employs the tabulated inverse distance values for the grid points.

III. DISCUSSION

In the following, several applications of the algorithm are presented. We start with a simple test example, and follow with the analysis of more complex geometries.

A. Example: Point charge near a conducting island

As an instructive example and as a test case for the algorithm, a $32\times32\times132$ grid was setup with one square metallic island in the lower region, while an external charge is placed at different positions away from the island surface and directly over its center (see inset of Fig. 2). The total dimensions of the grid in real space were taken to be $L_x=1$ [in units as per Eq. (8)], and accordingly $L_y=1$ and $L_z=4.2$ for equal grid spacing.

We calculate the interaction potential experienced by the point charge in the presence of the island. The results are shown in Fig. 2. For the case of a neutral island, close to the surface, the potential approaches that produced by the image charge of an infinite plane ($\sim 1/r$), while further away from the island, the potential approaches asymptotically the form

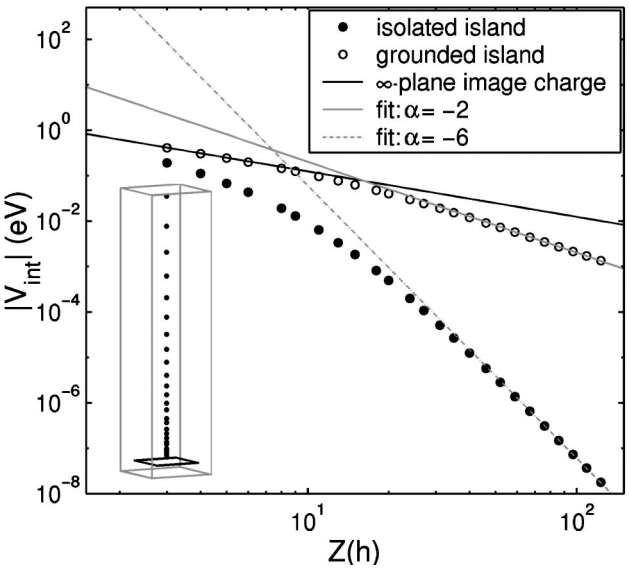

FIG. 2. Calculated interaction potential energy of a point charge ($q=1[e]$) with a finite size conducting plane. The grid configuration is shown to scale in the inset: the total block size is $32\times32\times132$, indicated by the gray box lines; positions of the point charge are indicated by the black dots in the inset, a set of locations vertically away from the metallic plane which is shown at the bottom by the black line (note that closest point charge to island distance is $3h$, three grid spacings). Shown are two configurations: neutral isolated island (filled circles) and grounded island (empty circles). Gray lines indicate different power law dependencies $\propto z^{\alpha}$.

of an induced quadrupole interaction potential ($\sim 1/r^6$) [9].

The calculation was done also for a grounded island. In this case, one obtains the limit of an infinite plane at short distances ($\sim 1/r$), while further away from the island the dependence weakens to $\sim 1/r^2$ as expected [10]. As a reference, the interaction potential in the presence of an infinite plane is shown (solid line in Fig. 2). The finite size of the island clearly reduces the interaction at large distances. Overall, it is interesting to see that one obtains exactly what is expected, but more importantly, the algorithm already gives useful results for rather small grid dimensions.

B. Example: Point charge interacting with an array of islands

Lithographically, an array of conducting islands can be separated from a two-dimensional electron gas by an insulating layer, as in the experiments with spatially modulated two-dimensional electron gases in semiconductors [2]. Considering the electron gas as a Fermi liquid, the interaction of a single electron (or single quasiparticle) with the conducting islands nearby is an important element of the physics of this problem since this interaction will clearly modify the dynamical behavior of the system [1]. Figure 3 shows the sample geometry used in this example.

With the test charge hovering over the center of one island and considering the conducting islands either grounded or isolated (uncharged), the calculated charge distribution and the potential in the plane of the islands are shown in Fig. 4; the grounded case can be understood as that of an island where hopping onto and off the island is allowed via a tun-

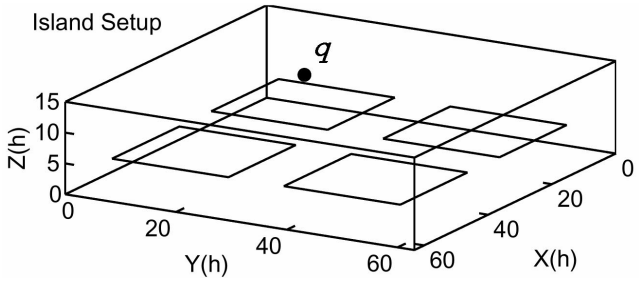

FIG. 3. Interacting point charge ($q=+1$) with an array of four islands in a plane underneath the point charge: a $64\times64\times16$ (box) cell with open boundaries was setup; its dimensions are $L_x=L_y=1$, $L_z=16h=0.25$ [units as per Eq. (8)]. The separation of the external charge from the island plane is $5h=5/64=0.078$.

neling channel from an external charge reservoir. A few points should be stressed: first, note that the variations of the potential in the plane of islands in Fig. 4 for the case of isolated islands is about a factor 10 *larger* compared to the grounded case since the island potential is not fixed. Second, the isolated islands are indeed neutral within numerical accuracy, the sum over all charges Q_{tot} is zero, within the accuracy provided by the convergence parameter ε (see lower two plots in Fig. 4: total induced charge in the plane of the islands = all positive surface charge + all negative surface charge $\simeq 0.442-0.442\sim10^{-7}\sim\varepsilon$). Third, the induced negative charge in the case of neutral islands is clearly smaller compared to the grounded case, which is intuitively clear, since in the neutral case the negative charge needs to be compensated by an equal amount of opposite charge, and

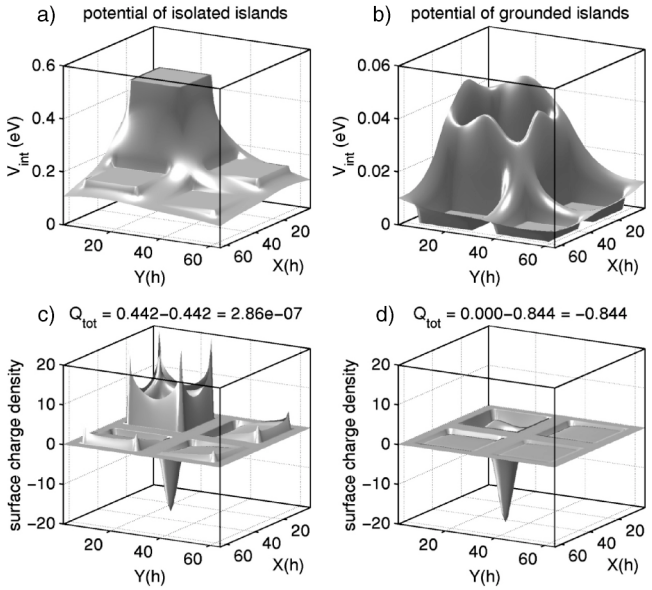

FIG. 4. Potential landscape and charge distribution *within* the plane of islands for the geometry in Fig. 3: the left (right) two graphs are for the case of neutral (grounded) islands, respectively. Note the quite different scale in the two potentials shown in plots (a) and (b). The induced surface charge density is shown in the plots (c) and (d) [in units as per Eq. (8)]; for better visualization the top (positive) and bottom (negative) surface charges of the islands are shown added up in a single plot.

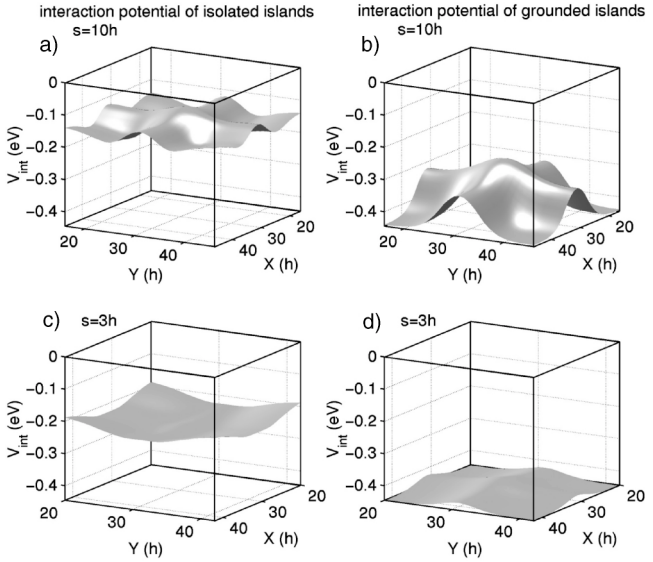

FIG. 5. Potential landscape of an external charge interacting with the array of islands. The geometry is the same as in Fig. 3 except for the separation between islands. Only the region of the four overlapping island corners is shown. The left two graphs (a) and (c) are for the case of isolated islands; the right two (b) and (d) for grounded islands; the upper two graphs are for an island separation s of $10h$ ($=10$ grid spacings), while the lower two graphs are for an island separation of $3h$.

this charge separation in the island costs energy. Therefore, the interaction with the external charge can be expected to be weaker for the isolated (neutral) islands, as is the case (see later, Fig. 5). Also note that in the neutral case the island corners exhibit accumulation of induced charges, as one would expect from the sharpness of the island corners. It is also interesting to observe that the induced charge never exceeds the external charge (in absolute value): at the maximum, it is just equal and opposite in sign (as for the case of the infinite plane).

As the external charge was displaced horizontally at a certain separation above the plane of the island, one effectively scans the potential landscapes for different geometries and different boundary conditions, as shown in Fig. 5. The isolated (neutral) islands show a clearly weaker modulation of the interaction potential. Furthermore, decreasing the island separation such that the gap between them is nearly closed, reduces most of the central modulation and smooths the potentials, as one would expect, and can be seen by comparing the upper two graphs in Fig. 5 with the lower two.

C. Mutually induced charge on STM tip

As a final example, the induced charges were calculated for the typical geometry of a metallic STM tip near a metallic array structure with the islands kept neutral; the geometry can be seen in panel (d) of Fig. 6. The parabolically shaped STM tip is maintained at a fixed potential ($V=1$) by an external source. The potential below the islands is weakened and shielded by the islands [panel (a)], while on the islands the potential is constant and is defined there by the constraint

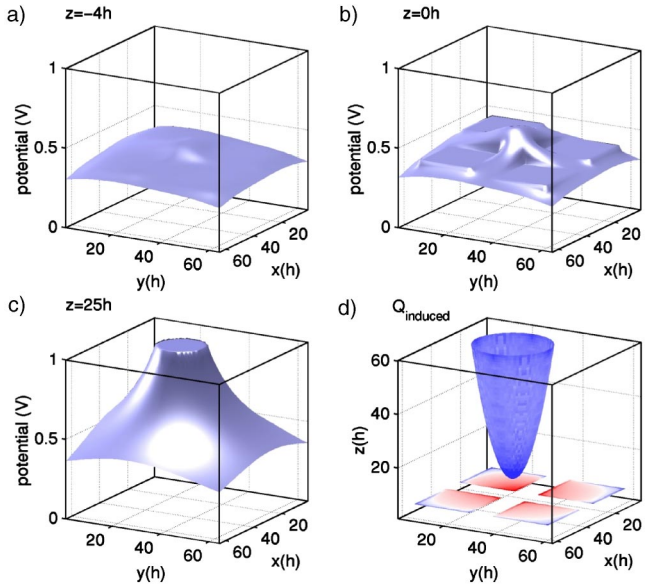

FIG. 6. (Color online) Potential and charge distribution for a conducting tip at potential $V=1$ above four isolated (neutral) islands; the distance between the plane of islands and the tip is $5h$. Panels (a)–(c) show xy slices in the potential distribution. Panel (a): potential just under the plane of islands ($z=-4h$ with respect to the plane of the islands); panel (b): potential right on the plane of islands ($z=0h$); and panel (c): potential on a plane above the tip ($z=25h$). Panel (d) is a contour plot of the charge distribution on the tip and on the overall neutral islands ($Q_{tot}^{islands}=+0.281+(-0.281)\simeq 10^{-10}$, i.e., nicely converged). The *extra* charge on the tip due to the presence of the islands is $+0.181$.

of neutrality [panel (b)]. Above the islands, in the region of the tip, the potential landscape (xy slice) has a circular plateau at the position of the tip with a potential of $V=1$ (the potential of the tip) and smoothly decays away from the tip [panel (c)]. Panel (d) indicates the charge distribution on the islands and on the tip; the charge on the tip is positive overall: $Q_{tip}^{0}=+4.01$ is the charge on the portion of the tip shown in the *absence* of the islands, and it gains a bit more of charge ($+0.181$) through the interaction with the metallic islands. The island with the tip right on top of it (right rear in inset) is the most polarized of all. The corner in the center is *negatively* charged, while the transition through the white region on the island surfaces in panel (d) indicates that the surface charge switches sign there, and that the outer region of the islands are positively charged. In addition, the lower island surfaces are also mostly positive, as one would expect. This compensates the negative charge induced by the tip and guarantees the neutrality of the islands (see caption for explicit numbers).

IV. SUMMARY

In summary, the electrostatic potential of complex metallic arrangements were calculated on a three-dimensional grid with an $O(h^6)$ algorithm. The algorithm presented here is a generalization of the relaxation techniques common in two-dimensional systems, properly set up to provide accurate and efficient calculations. The approach allows the study of arbitrary geometries and boundary conditions, as well as the self-consistent calculation of free and induced charges. This information, in turn, allows the calculation of the capacitance matrix of the system. Several examples illustrate the reliability and usefulness of the algorithm for obtaining potential landscapes of interest.

ACKNOWLEDGMENTS

We acknowledge support from NSF Grant No. NIRT 0103034, and the Condensed Matter and Surface Sciences Program at Ohio University.

[1] K. Likharev, Proc. IEEE **87**, 606 (1999).

[2] See, for example, D. Weiss, M. Roukes, A. Menschig, P. Grambow, K. von Klitzing, and G. Weimann, Phys. Rev. Lett. **66**, 2790 (1991).

[3] S. Teukolsky, W. Vetterling, W. Press, and B. Flannery, *Numerical Recipes in C*, 2nd ed. (Cambridge University Press, New York, 1993).

[4] James W. Demmel, *Applied Numerical Linear Algebra* (SIAM, Philadelphia, 1997)

[5] J. D. Jackson, *Classical Electrodynamics*, 3rd ed. (Wiley, New York, 1999).

[6] T. B. R. Coalson, *Encyclopedia of Computational Chemistry*, (Wiley, New York, 1998), Vol. 3, p. 2080.

[7] Calculating the external charges (e.g., that of an isolated electron) is not needed explicitly since known, but it serves as a nice self-check of the algorithm. As an example, the charge distribution around a free electron was calculated, introduced into the system as a δ charge (i.e., a source of $1/h^3$ on a single grid point). With nearest neighbor sites included because of the discreteness of the lattice, the total charge over these $1+6$ grid points correctly gave the overall charge up to numerical precision.

[8] When calculating an artificial charge at the outer boundary by assuming continued constant potential right at the border results in the constraint that the sum of charges from all grid points needs to approach zero. This was also nicely fulfilled up to a relative error of 10^{-7}, the order of the convergence parameter ε.

[9] The quadrupole dependence is obtained because the island is taken ideally thin (one grid layer) and therefore, out of symmetry of the chosen configuration, there is no dipole moment; with this, the far field $\sim 1/r^6$ dependence for a quadruple is obtained in a similar fashion as in Ref. [10].

[10] The far field $\sim 1/r^2$ dependence for a grounded conductor can be obtained by minimizing the energy of the probe charge in the presence of the charged conductor, $E=Q^2/2C+qQ/z$, where q is the probe charge, Q is the charge on the conductor of capacitance C, and z is their separation. The minimal energy yields $Q=-qC/z$, so that the potential on q is then $qQ/z=-q^2C/z^2$.